Pre-Processing Techniques and Noise Distribution Learning in Magnetic Resonance Imaging

Final Project

ECE 783 Digital Image Processing

Michael Evans

Due: 04 December 2025

Submitted: 04 December 2025

Abstract.

Alzheimer's disease (AD), defined by the accumulation of amyloid plaques and tau tangles in the brain can be diagnosed with biomarkers obtained from PET scans or CSF proteomics. However, such methods are expensive and invasive, leading to most AD diagnoses being made based on cognitive tests and evidence of atrophy in the medial temporal lobe structures, such as the hippocampus and amygdala. Machine and deep learning architectures such as convolutional neural networks (CNNs) have seen great success in diagnosing AD from magnetic resonance imaging (MRI). Moreover, current studies have begun to outperform methods typically used in practice for classifying hard to detect subgroups (atypical AD). However, the input scans for such models rely heavily on pre-processing, and the accurate detection of AD is reliant on the signal-to-noise ratio (SNR), a result of instrument-related parameters such as magnetic field strength. In this project, we first build a dataset suitable for AD binary classification and implement contemporary pre-processing methods found in the literature. Next, we introduce additive noise to the pre-processed images sampled from the distribution MRI is most vulnerable to during acquisition time. Finally, we apply non-local means filtering to denoise the MR images and plot the residual distribution of the noise. Our denoising algorithm achieves a SNR percent increase of up to 39.8%, and we show experimentally that the Rician distribution is approximately Gaussian for high SNR.

[This space intentionally left blank.]

Introduction.

Alzheimer's disease (AD) is a progressive neurodegenerative condition and the most common cause of dementia in older adults. The diagnosis of AD is generally based on history-taking and memory tests given in clinics, rather than with the use of biomarkers taken from PET scans or lumbar puncture. This can make it difficult to obtain an objective diagnosis, causing specialists working in memory clinics to have lowered levels of diagnostic agreement [1]. However, the application of deep learning to automated classification of AD has recently gained considerable attention, following progress in neuroimaging acquisition [2]. Deep learning architectures such as convolutional neural networks (CNNs) rely heavily on the pre-processing of the input scans and are sensitive to noise [3]. Thus, a great deal of effort has gone into developing a common standard for pre-processing MR images for computer vision tasks, such as fMRIPrep [4]. In this project, we build a dataset of 257 AD and 293 cognitively normal (CN) patients from the Alzheimer's Disease Neuroimaging Initiative (ADNI) and apply standardized pre-processing techniques suitable for AD classification. We apply intensity non-uniformity (INU) correction, skull-stripping, spatial normalization, and brain tissue segmentation with the fMRIPrep pipeline [4]. Next, we introduce additive noise sampled from the Rician distribution to the magnitude MR image and calculate SNR. A non-local (NL) means filter is then applied to the corrupted scans to denoise the images. Though the noise distribution is known, we plot the residuals of the restored scans as a denoising metric and to interpret the effects of increasing the standard deviation of the sampled noise.

Technical Discussion.

Data.

Data used in this project is limited to T1 weighted deidentified MRI scans obtained from the ADNI data set [5]. We collected 257 patients diagnosed with AD and 293 CN patients. AD patients must have evidence of AD pathology based on PET scan, CSF analysis, or autopsy neuropathology results. CN patients were filtered using the diagnosis labels assigned to patients at the initial screening visit. The raw dicom files from ADNI were first converted to nifti using the dicm2nii [6] tool in MATLAB. Next, each patient was converted into the BIDS [7] format and pre-processed with fMRIPrep.

Data Pre-processing.

In this section, we outline the data pre-processing steps performed as part of the fMRIPrep pipeline. Signal intensity measured from homogeneous tissue is rarely uniform and varies across the image. This nonuniformity is usually attributed to "poor radio frequency (RF) coil uniformity, gradient-driven eddy currents, and patient anatomy both inside and outside the field of view" [8]. To correct this issue, the intensity histogram of the image is repeatedly sharpened by deconvolving by a Gaussian (assumed Gaussian can model bias), then smoothed with a B-spline [9]. This is referred to as intensity non-uniformity correction and is the first process applied to the scans.

Next, skull-stripping is implemented to eliminate non-brain tissues from the MR images using template-based registration to OASIS [10]. This is an essential step before performing normalization to the spatial template images and is required for de-identification of subjects [11]. Then, registration to a common reference space is performed to establish a one-to-one correspondence between the brains of different individuals [12]. Lastly, brain tissue segmentation is performed to segment the 3D image into different tissue types (Grey/White matter, CSF) [13]. We use this output as the reference image for modeling the noise and calculating SNR in a later section. This pipeline was run on all 550 patients with 8 GPU cores in parallel batch jobs submitted through slurm on the Wahab shared computing cluster at Old Dominion University.

Additive Rician Noise.

Rician noise is the most common form of noise in MR magnitude images [14] and is created by taking the magnitude of a bivariate normal distribution:

$$\sqrt{(signal_{\mathbb{R}} + noise_{Gaussian})^2 + (signal_i + noise_{Gaussian})^2} : \mu = 0;\ \sigma_{\mathbb{R}} = \sigma_i \qquad (1)$$

The Rician distribution of a noisy MRI magnitude image has the following PDF:

$$p_M(M) = \frac{M}{\sigma^2} exp\,(-\left(\frac{M^2 + A^2}{2\sigma^2}\right)) I_0\left(\frac{A * M}{\sigma^2}\right) \quad (2)$$

Where M is the measured pixel intensity, A is the image pixel intensity without noise, and I_0 is the modified zeroth order Bessel function [5, 15]. This type of noise is inherent to MR images due to the signal at acquisition time being measured through a quadrature detector, reading in

both real and imaginary signals in k-space (Fourier space) [14]. We assume the noise in both signals is Gaussian with zero mean and the distributions are uncorrelated, due to the complex Fourier transform applied to the k-space being linear and orthogonal preserving the Gaussian characteristics [8]. Magnitude images are created by calculating the magnitude pixel by pixel from the real and imaginary images [8]. This nonlinear mapping to create the magnitude image causes the noise distribution to no longer be Gaussian. This is called Rician noise [8].

Non-local Means Denoising.

Unlike local meaning filters, non-local (NL) mean filtering takes the mean of all pixels in the image, taking advantage of the natural redundancy of information in images [16]. The central idea of using NL means filtering is that similar pixels are not guaranteed to be close in space [17]. Therefore, it is better to search a large portion of the image for pixels resembling the one we want to denoise [17]. The restored intensity $NL(v)(i)$ of the voxel i is a weighted average of all voxel intensities in the image I:

$$NL(v)(i) = \sum_{j \in I} w(i,j)v(j) \tag{3}$$

Where v is the intensity function and $w(i,j)$ is the weight assigned to $v(j)$ in the restoration of voxel i [16]. This follows from the impact of averaging M signals on the SNR:

$$\bar{p}(x,y) = \frac{M^2 s^2(x,y)}{ME\{N^2(x,y)\}} \tag{4}$$

Where the signal increases with the square of M, and noise linearly.

Discussion of Results.

Figure [N1] shows the reference image of a T1 weighted MR image in the axial plane after pre-processing with fMRIPrep. This output image is assumed to have no or minimal noise and an infinite SNR, instead of estimating the true SNR which is out of scope for this project. Figures [N2-N5] are the result of applying equation (1) to the reference magnitude MR image, creating a noisy magnitude MR image with the PDF defined in equation (2). Table [T1] displays the SNR of each non-zero σ, which defines the standard deviation of both Gaussian distributions sampled from in equation (1). In effect, this parameter allows to adjust the level of additive

Rician noise in the corrupted images [N2-N5]. As σ increases, the amount of noise in the degraded image increase, and the SNR decreases.

Next, we apply NL means filtering from equation (3) to denoise the corrupted images. Figure [D1] is identical to the reference magnitude MR image [N1] since $\sigma = 0$. Figures [D2-D5] are the restored images after applying NL means filtering. Due to the level of redundant information in the reference scan, the results of this denoising algorithm are very impressive. This filtering technique takes advantage of the properties of image averaging defined in equation (4), where similar pixels are averaged if their neighboring pixels have a low mean square error defined by a patch size parameter. Since MR images have similar pixels within a defined patch size, high averaging of the signals results in impressive performance. Table [T1] contains the SNR of the corrupted and restored images, with percent increase that rises with the noise.

Lastly, we plot the residual of the error between the reference image [N1] against each restored image [D2-D5]. Figure [R1] is the residual error of the entire image, even the areas of no signal. It is standard practice to only include the regions of brain tissue to accurately measure performance of the denoising filter, shown in figure [R2]. The peaks around 0 in figure [R1] indicate strong performance from the filter, as many regions have no error between the reference and denoised images. However, the larger peaks evident in this figure highlight the error in the regions of no signal, representing air during MRI acquisition. Therefore, measuring the residual of an area with no signal becomes ineffectual. Instead, figure [R2] plots the residual in only the regions with signal (brain tissue) and models the noise distribution much closer. Residuals with high SNR approximate the Gaussian distribution, while noise from the lower SNR images appear more Rician, as expected from [4]. Residuals of high performing denoising filters should follow a reduced form of the target distribution, evident in figure [R2]. While the true distribution of noise was known in this case, this tool can reveal properties of the noise if unknown.

Summary.

In this project, we built a dataset suitable for future deep learning based AD classification and implemented common pre-processing methods to create reference magnitude MR images. Then, we degraded the reference images with additive Rician noise created from the magnitude of a circularly symmetric bivariate normal random variable, commonly introduced as Gaussian

noise in the real and imaginary signals during MRI acquisition. Finally, we apply non-local means filtering to denoise the MR images and plot the residual error.

Results.

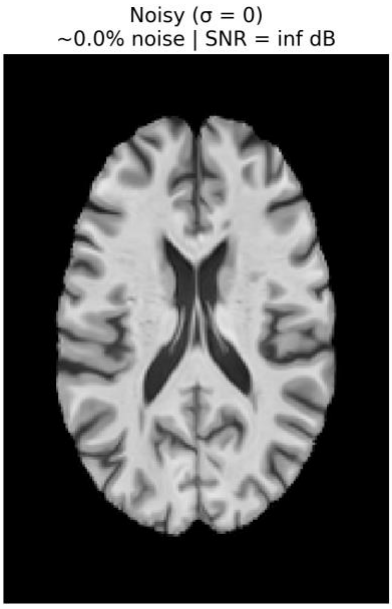

[N1]

[N2]

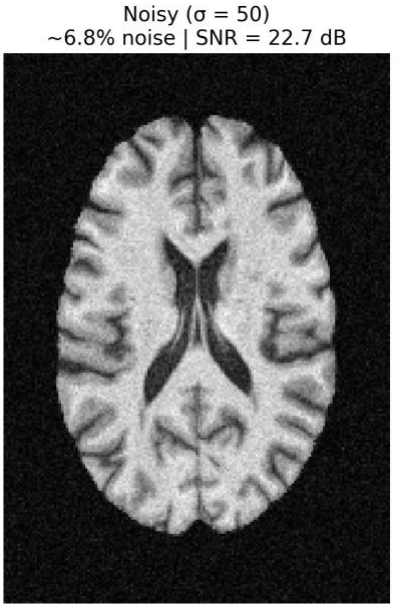

[N3]

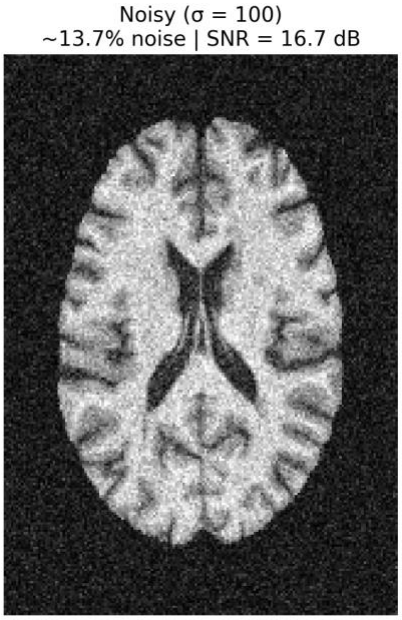

[N4]

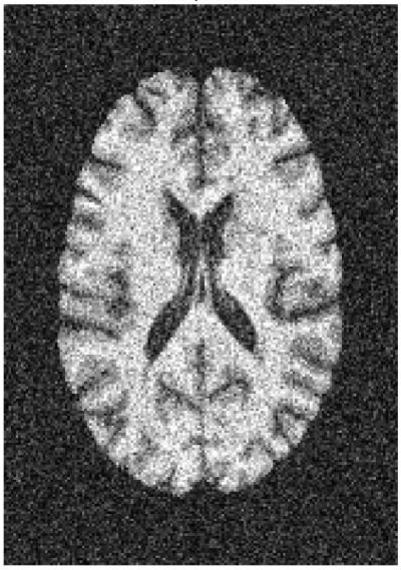

[N5]

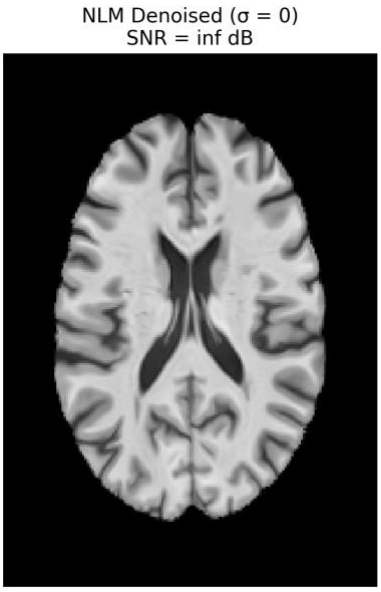

[D1]

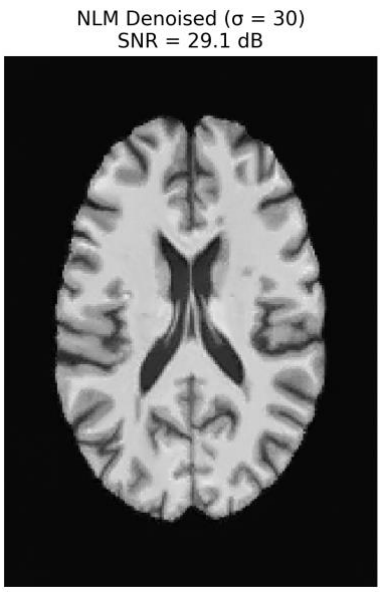

[D2]

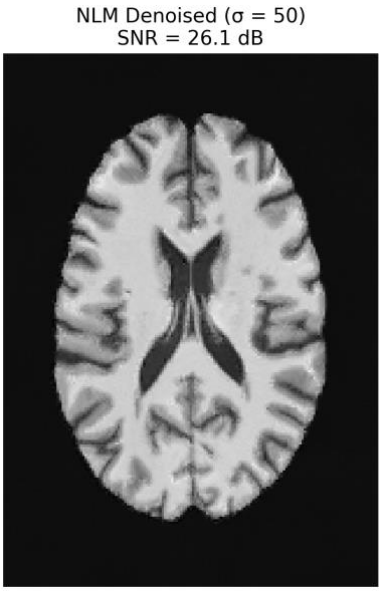

[D3]

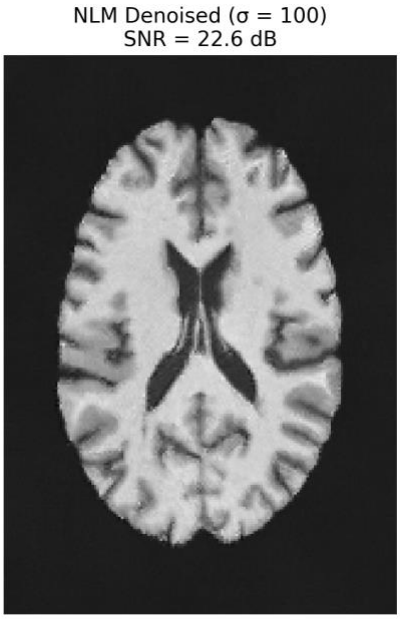

[D4]

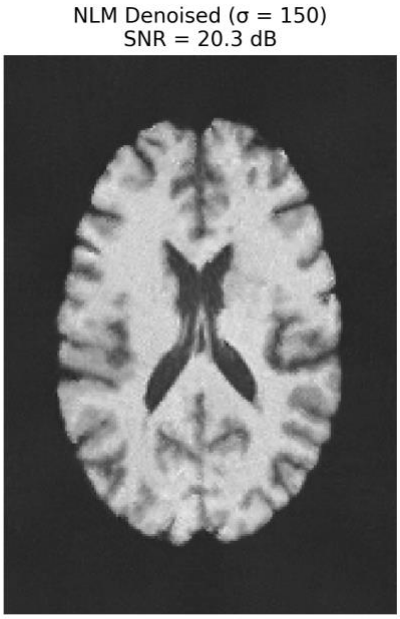

[D5]

Table [T1]	$\boldsymbol{\sigma = 30}$	$\boldsymbol{\sigma = 50}$	$\boldsymbol{\sigma = 100}$	$\boldsymbol{\sigma = 150}$
Noisy SNR	27.2 dB	22.8 dB	16.8 dB	13.3 dB
Denoised SNR	29.1 dB	26.1 dB	22.6 dB	19.9 dB
% Increase	6.7%	13.5%	29.4%	39.8%

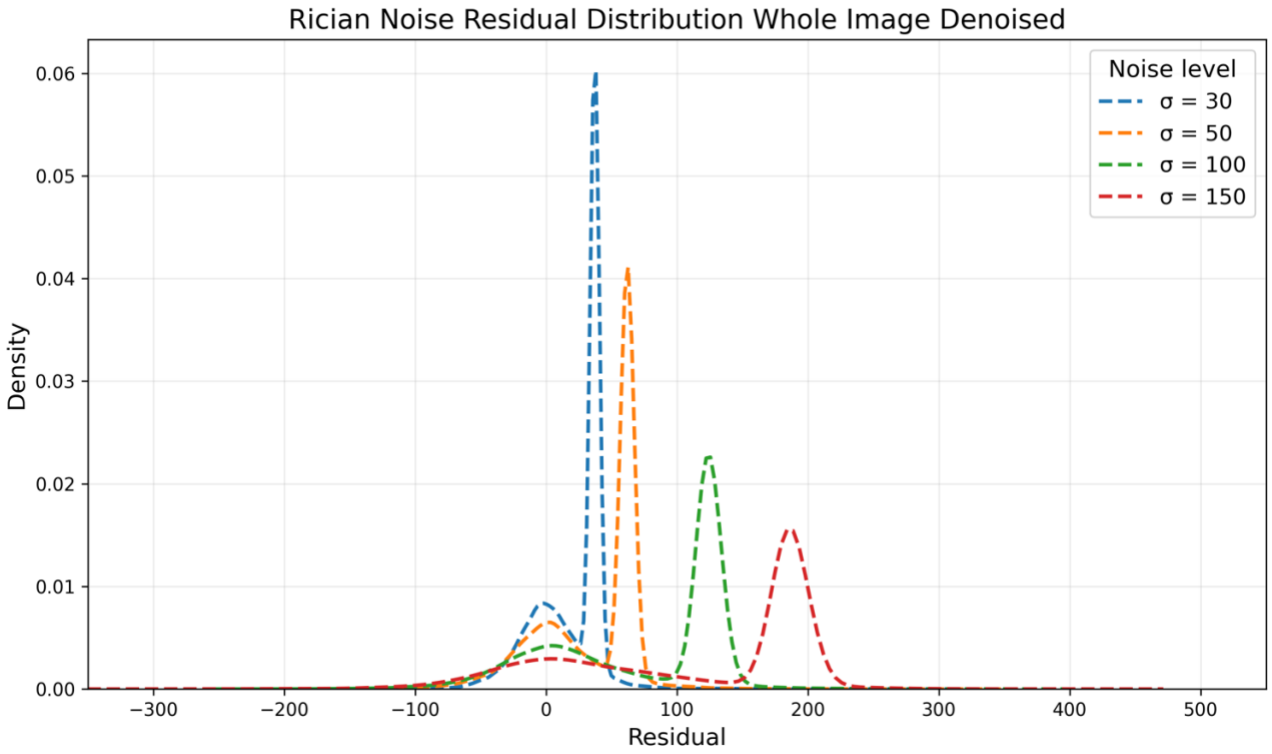
Rician Noise Residual Distribution Whole Image Denoised
Noise level
σ = 30
σ = 50
σ = 100
σ = 150
Density
Residual
0.00
0.01
0.02
0.03
0.04
0.05
0.06
−300
−200
−100
0
100
200
300
400
500

[R1]

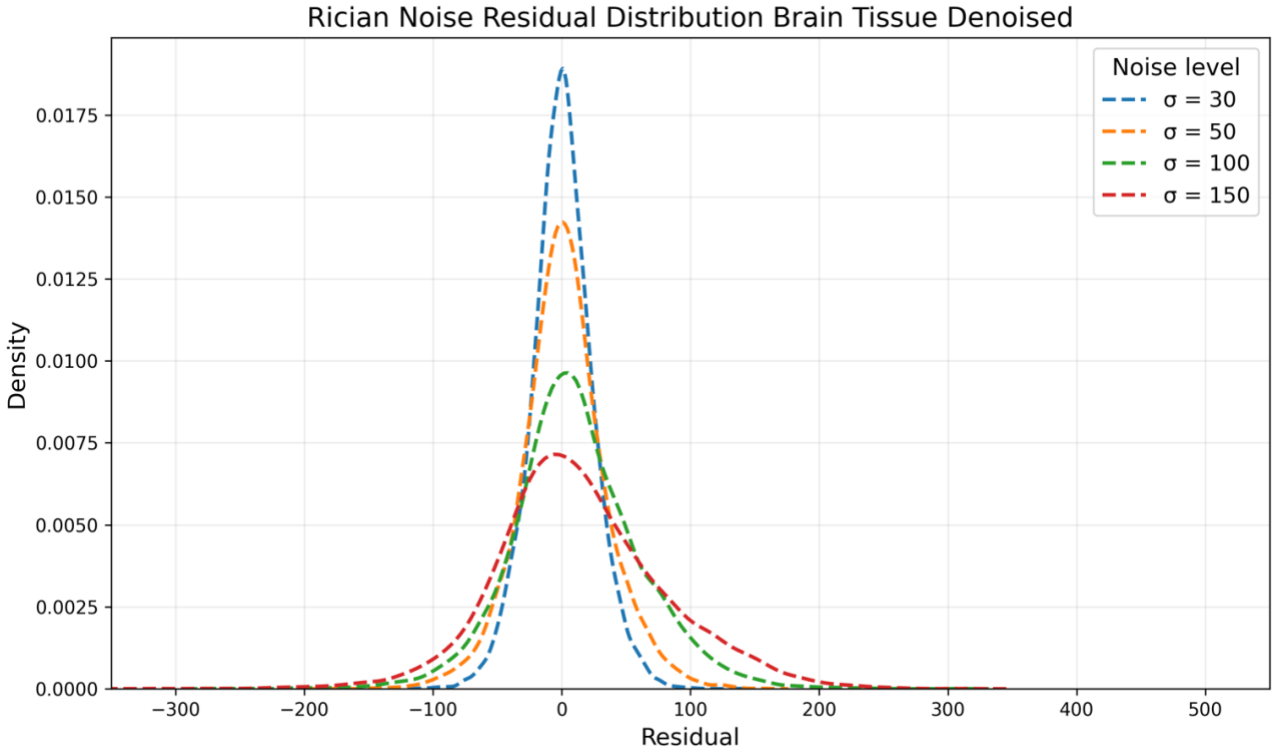
Rician Noise Residual Distribution Brain Tissue Denoised
Noise level
σ = 30
σ = 50
σ = 100
σ = 150
Density
Residual
0.0000
0.0025
0.0050
0.0075
0.0100
0.0125
0.0150
0.0175
−300
−200
−100
0
100
200
300
400
500

[R2]

References.

[1] An, Ning, et al. "Deep ensemble learning for Alzheimer's disease classification." *Journal of biomedical informatics* 105 (2020): 103411.

[2] Jo, Taeho, Kwangsik Nho, and Andrew J. Saykin. "Deep learning in Alzheimer's disease: diagnostic classification and prognostic prediction using neuroimaging data." Frontiers in aging neuroscience 11 (2019): 220.

[3] Zhou, Xiao, et al. "Enhancing magnetic resonance imaging-driven Alzheimer's disease classification performance using generative adversarial learning." *Alzheimer's research & therapy* 13.1 (2021): 1-11.

[4] Esteban, Oscar, et al. "fMRIPrep: a robust preprocessing pipeline for functional MRI." *Nature methods* 16.1 (2019): 111-116.

[5] Petersen, Ronald Carl, et al. "Alzheimer's disease Neuroimaging Initiative (ADNI) clinical characterization." Neurology 74.3 (2010): 201-209.

[6] Li, Xiangrui, et al. "The first step for neuroimaging data analysis: DICOM to NIfTI conversion." *Journal of neuroscience methods* 264 (2016): 47-56.

[7] Gorgolewski, Krzysztof J., et al. "The brain imaging data structure, a format for organizing and describing outputs of neuroimaging experiments." *Scientific data* 3.1 (2016): 1-9.

[8] Sled JG, Zijdenbos AP, Evans AC. A nonparametric method for automatic correction of intensity nonuniformity in MRI data. IEEE Trans Med Imaging. 1998 Feb;17(1):87-97. doi: 10.1109/42.668698. PMID: 9617910.

[9] ANTsX. "N4BiasFieldCorrection." *GitHub*, 12 Jan. 2021, github.com/ANTsX/ANTs/wiki/N4BiasFieldCorrection.

[10] Marcus DS, Wang TH, Parker J, Csernansky JG, Morris JC, Buckner RL. Open Access Series of Imaging Studies (OASIS): cross-sectional MRI data in young, middle aged, nondemented, and demented older adults. J Cogn Neurosci. 2007 Sep;19(9):1498-507. doi: 10.1162/jocn.2007.19.9.1498. PMID: 17714011.

[11] Fischmeister, F. Ph S., et al. "The benefits of skull stripping in the normalization of clinical fMRI data." *NeuroImage: Clinical* 3 (2013): 369-380.

[12] Crinion, Jenny, et al. "Spatial normalization of lesioned brains: performance evaluation and impact on fMRI analyses." *Neuroimage* 37.3 (2007): 866-875.

[13] "FAST." *Mit.edu*, 2017, web.mit.edu/fsl_v5.0.10/fsl/doc/wiki/FAST.html.

[14] Gudbjartsson, Hákon, and Samuel Patz. "The Rician distribution of noisy MRI data." *Magnetic resonance in medicine* 34.6 (1995): 910-914.

[15] Bowman, Frank. *Introduction to Bessel functions*. Courier Corporation, 2012.

[16] Coupé, Pierrick, Pierre Yger, and Christian Barillot. "Fast non local means denoising for 3D MR images." *International conference on medical image computing and computer-assisted intervention*. Berlin, Heidelberg: Springer Berlin Heidelberg, 2006.

[17] Buades, Antoni, Bartomeu Coll, and Jean-Michel Morel. "Non-local means denoising." Image processing on line 1 (2011): 208-212.